

# TSDASeg: A Two-Stage Model with Direct Alignment for Interactive Point Cloud Segmentation

Chade Li<sup>1,2</sup> Pengju Zhang<sup>1</sup> Yihong Wu<sup>1,2\*</sup>  
<sup>1</sup>State Key Laboratory of Multimodal Artificial Intelligence,  
 Institute of Automation, Chinese Academy of Sciences

<sup>2</sup>School of Artificial Intelligence,  
 University of Chinese Academy of Sciences  
 lichade2021@ia.ac.cn, {pengju.zhang@ia, yhwu@nlpr.ia}.ac.cn

## Abstract

The rapid advancement of 3D vision-language models (VLMs) has spurred significant interest in interactive point cloud processing tasks, particularly for real-world applications. However, existing methods often underperform in point-level tasks, such as segmentation, due to missing direct 3D-text alignment, limiting their ability to link local 3D features with textual context. To solve this problem, we propose **TSDASeg**, a Two-Stage model coupled with a **Direct cross-modal Alignment module** and memory module for interactive point cloud **Segmentation**. We introduce the direct cross-modal alignment module to establish explicit alignment between 3D point clouds and textual/2D image data. Within the memory module, we employ multiple dedicated memory banks to separately store text features, visual features, and their cross-modal correspondence mappings. These memory banks are dynamically leveraged through self-attention and cross-attention mechanisms to update scene-specific features based on prior stored data, effectively addressing inconsistencies in interactive segmentation results across diverse scenarios. Experiments conducted on multiple 3D instruction, reference, and semantic segmentation datasets demonstrate that the proposed method achieves state-of-the-art performance.

## 1. Introduction

With the development of technologies such as LLMs and 2D VFMs, text-guided interactive 3D segmentation tasks are gradually becoming a hot research topic due to their practical significance. The goal of this task is to enable users to segment 3D objects or whole scenes using natural

\*Corresponding Author

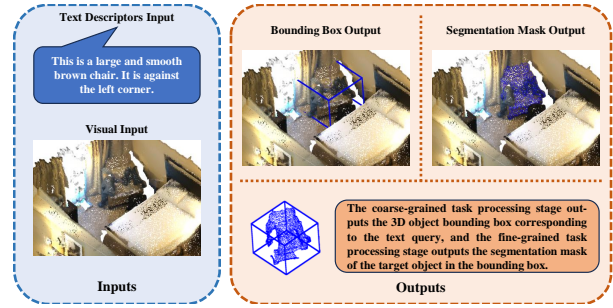


Figure 1. The inputs and outputs of the proposed two-stage detection-segmentation model.

language inputs. Existing methods [12, 25, 34, 42, 52, 56] typically leverage the capabilities of LLMs to interpret textual inputs, while employing the CLIP model [36] to establish cross-modal associations between 2D images and text. Alternatively, these methods utilize VFMs to directly process 2D visual data, relying on the camera’s intrinsic and extrinsic parameters to establish geometric correspondences between 2D projections and 3D coordinates, thereby indirectly inferring 3D point cloud semantics through multi-view fusion.

PointCLIP [52] further extends the understanding of 3D data by utilizing the ideas of CLIP [36] to construct an alignment of 2D images with text data. The CLIP [36] trains the image encoder and the text encoder through contrastive learning, so that the matching image and text pairs are closer in the embedding space, and vice versa. Seal [25] utilizes VFMs to segment different automotive point cloud sequences by distilling semantic perceptions from VFMs to point clouds on camera views through hyperpixel-driven contrastive learning. The fine-grained segmentation task requires the model to have the ability to recognize and dis-

tinguish the tiny structures and changes inside the target object, which not only requires the model to have a deep understanding of the 3D shapes, but also the ability to capture local details and text information. The above existing methods [25, 52] tend to construct an indirect alignment of the 3D point cloud with other data by using the 2D image as intermediate data, which is highly susceptible to internal and external parameter computation errors as well as mismatches between the 2D pixels and the 3D points. Therefore, the existing methods are unable to establish a stable and accurate coordinate correspondence between the 3D point cloud and the 2D image, thus failing to meet the capability requirements of fine-grained tasks at the point level.

To address the above problems, we introduce TSDASeg, a two-stage model for interactive point cloud segmentation, coupled with proposed Direct Cross-Modal Alignment module and Memory Module. Specifically, we first use the cross-modal attention module to simultaneously direct align 3D features with text features and 2D features. And at the same time, we use the idea of contrastive learning for 2D features and text features to further constrain the alignment of 3D features with other features. After obtaining the aligned visual features, the features are updated and processed by a multilayer multiscale Transformer block and passed through a detection header to obtain a 3D box for a specific text query input. In addition, we introduce a Memory Module for storing text-visual feature pairs within the bounding box and storing them into the memory bank with weights assigned according to their confidence levels. This allows the network to fully utilize the existing training knowledge when processing subsequent scenes, so as to compensate for the inconsistency of interactive segmentation results from different scenes. Then, we input the text query and the updated features corresponding to the 3D points in the 3D box into the introduced Memory Module for feature processing, and use the real-time iterative updated binary classifier to generate the final segmentation result. Experimental results on indoor and outdoor datasets for a variety of downstream tasks show that our method outperforms existing methods. The main contributions of our work can be summarized as follows:

- We propose an innovative interactive point cloud segmentation network that first coarsely detects 3D objects and then finely segments the corresponding query objects.
- We present a Direct Cross-Modal Alignment module between 3D point clouds and other inputs, directly aligning the 3D features with other data using proposed attention module, with constraints using contrastive learning.
- We introduce a Memory Module that stores multimodal visual-text feature pairs, enabling the network to dynamically leverage prior knowledge during new scene processing, thereby improving cross-scenario consistency.
- Extensive experiments on several indoor and outdoor

datasets containing 3D instruction, referring, and semantic segmentation tasks demonstrate that the proposed method has excellent interactive segmentation results, validating the effectiveness and robustness of our work.

## 2. Related Work

In this section, we briefly overview related works of deep learning on point cloud segmentation and text-guided interactive 3D segmentation.

### 2.1. Deep Learning on Point Cloud Segmentation

In recent years, deep learning-based methods for point cloud segmentation have advanced significantly, driven by innovations in network architectures and feature aggregation strategies. According to the network principle and the data formats handled, the commonly used 3D point cloud segmentation methods can be categorized as follows: voxel-based methods [6, 9], projection-based methods [20, 44, 53], 2D processing guided methods [7, 16, 23, 27, 31], MLP-based methods [13, 22, 32, 33], point convolution-based methods [24, 39, 40], and attention-based methods [5, 10, 17–19, 26, 28, 29, 37, 38, 43, 46, 47, 55].

Voxel-based methods discretize 3D space into regular grids to enable 3D convolution, but often have difficult trade-offs between resolution and efficiency. Projection-based methods convert 3D points into 2D representations and utilize well-established 2D CNN architectures for feature learning. Methods that incorporate 2D processing borrow 2D segmentation networks or 2D VFMs to alleviate the computational resources required for training, but suffer from low accuracy due to issues such as domain differences. MLP-based methods (e.g., PointNet [32] and its successors) can run directly on the original point cloud, and tend to be effective in improving the sensory field while limiting computational resources. Point convolution methods excel in capturing fine-grained local geometry and handling irregular point distributions through deformable kernels, though they often face challenges in computational efficiency and parameter sensitivity when scaling to large-scale or sparse point clouds. Recent advances in attention mechanism methods [5, 10, 17–19, 21, 26, 28, 29, 37, 38, 43, 46, 47, 55] including Transformer and Mamba-like networks further improve the accuracy of segmentation tasks.

Based on the current application of deep learning in point cloud segmentation, we still choose the attention network based on Transformer as the backbone.

### 2.2. Text-Guided Interactive 3D Segmentation

The goal of the text-guided interactive 3D segmentation task is to enable users to manipulate and segment 3D objects or scenes using natural language commands or prompts. This task is critical for applications such as autonomous

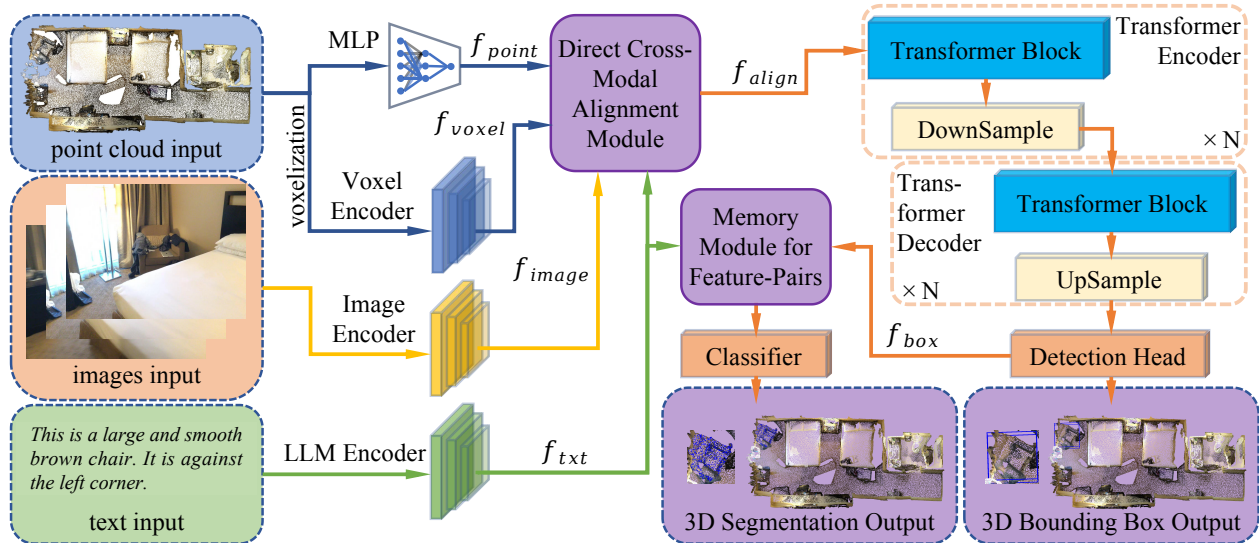


Figure 2. A general overview of the proposed network. Given point cloud, images, and text input, the point cloud is first voxelized. Then we use MLP, voxel encoder, image encoder, and LLM encoder to extract four distinct feature representations:  $f_{point}$ ,  $f_{voxel}$ ,  $f_{image}$ , and  $f_{txt}$ . These heterogeneous features are then unified via our novel Direct Cross-Modal Alignment (DCMA) module to generate aligned features  $f_{align}$ . Subsequently, the aligned features undergo refinement through a multi-layer Transformer encoder-decoder architecture. Following this, a detection head produces bounding box predictions and extracts point-wise features  $f_{box}$  within each detected region. The  $f_{box}$  and  $f_{txt}$  are jointly fed into the proposed Memory Module, which leverages stored cross-modal priors. Finally, an auxiliary classifier processes the fused features to yield the interactive segmentation results.

driving, robotics, and augmented reality, which require accurate 3D scene understanding and dynamic editing. By utilizing multimodal inputs (e.g., text, images, and point clouds), these methods [1, 4, 11, 14, 15, 35, 45, 49, 54] connect semantic linguistic descriptions with geometric 3D representations, improving usability and accuracy in complex environments.

Moreover, interactive 3D segmentation can also be categorized into referring segmentation and instruction segmentation. In the 3D referring segmentation task, given a textual input containing an explicit category word, the model needs to output the 3D point cloud mask of the corresponding object. And 3D instruction segmentation is introduced in SegPoint [12], unlike the former task, where the text input in this task does not contain a specific category word, and instead, it is a description of the function of the target object. Both tasks require the network not only capable of recognizing and responding to textual inputs, but also having a strong comprehension of the text, which requires the model’s reasoning ability and access to knowledge of the world. However, the current accuracy on the existing task datasets is insufficient which is nowhere near the level of accuracy in semantic segmentations. Furthermore, the direct alignment between 3D point cloud and other data is still greatly lacked.

In this regard, we design a Direct Cross-Modal Alignment module between 3D features and other modality fea-

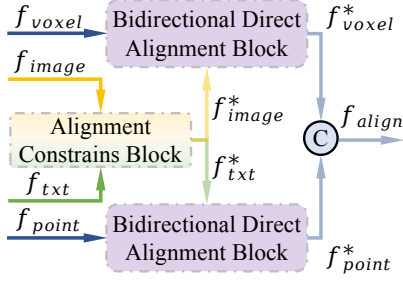
tures to mitigate the effect of errors caused by internal and external parametric computation or the lack of accurate 2D-3D correspondence. And we propose a Memory Module to enhance the network’s knowledge of text-to-visual mapping, thus improving the network’s sensitivity to text-visual correspondences and the accuracy of interactive segmentation tasks.

### 3. Methodology

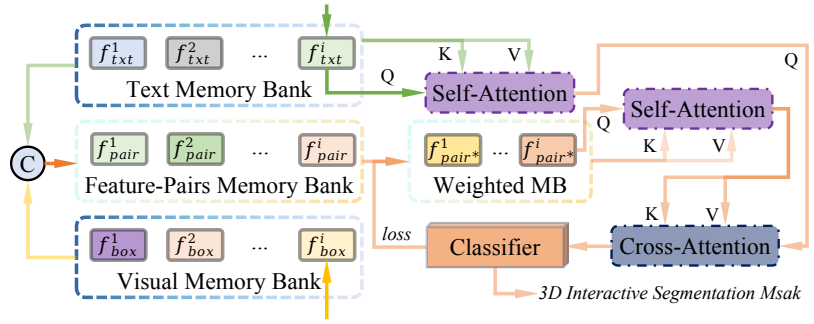
In this section, we first present a general overview of the proposed network framework in Section 3.1. Then we introduce the two important modules of our proposal, Direct Cross-Modal Alignment and Memory Module for Feature Pairs, respectively, in Sections 3.2 and 3.3 in turn. Finally, we show the objective function of the proposed method in Section 3.4.

#### 3.1. Framework Overview

The framework of our two-stage interactive point cloud segmentation network with a Direct Cross-Modal Alignment module and a Memory Module is shown in Figure 2. First, we input the point cloud, the corresponding 2D image, and the text query. Then, we apply the designed 3D and 2D Transformer encoders to extract features from the input point cloud and corresponding image, respectively, and generate text features using LLaMa2-7B [41] to the text query input after text vectorization. Besides, we additionally vox-



(a) Framework of the proposed Direct Cross-Modal Alignment module.



(b) Framework of the proposed Memory Module for feature pairs.

Figure 3. Visualization of two important modules in the proposed DSDASeg.

elize the point cloud input and apply the voxel Transformer encoder to get the voxel features. After that, we apply the proposed Direct Cross-Modal Alignment module to align the multimodal features.

After obtaining the aligned features, the features continue to be updated through a multi-layer multi-scale Transformer network. Subsequently, we obtain the bounding box of the target object corresponding to the text query in 3D space through a detection header. The 3D point features within the detected bounding boxes and their associated text query features are jointly input into our proposed Memory Module. Leveraging high-confidence text-visual feature pairs stored in the Memory Module, we iteratively train a binary classifier through an extra loss function. This enables progressive refinement from coarse 3D bounding boxes to precise segmentation results, establishing our framework as a two-stage pipeline, as illustrated in Figure 1.

### 3.2. Direct Cross-Modal Alignment

The proposed Direct Cross-Modal Alignment (DCMA) module is divided into two main parts, named the Alignment Constrains Block and the Bidirectional Direct Alignment Block, as shown in Figure 3a: the former applies constraints between text features and 2D image features that are directly aligned to the 3D features to ensure the accuracy of the feature alignment process; the latter uses the proposed bidirectional cross-modal attention mechanism to directly align 3D features with other modal features.

**Alignment Constrain Block.** In order to make the subsequent 3D features have the correct correspondence with other modal features in the alignment process, we apply independent encoders to the image features  $f_{image}$  and text features  $f_{txt}$  first for feature processing and mapping, so that the matched image features and text features are closer together in the embedding space, as shown in Equation (1).

$$f_{image}^*, f_{txt}^* = Encoders_{ind}(f_{image}, f_{txt}). \quad (1)$$

For the independent encoder of image and text features used above, we train these encoders by the following process. We select at most one pair of matching image and text data for each scene in the experimental dataset, encode them using independent encoders, obtain the remapped image and text features, and compute the cosine similarity between all image and text features to form a similarity matrix. Then a symmetric cross-entropy loss function is introduced to maximize the similarity scores of correct matching pairs (the elements on the diagonal) and minimize the similarity scores of incorrect matching pairs (the off-diagonal elements). This contrastive learning strategy forces the encoder to achieve alignment of 2D and textual representations, effectively mapping the corresponding textual and image features to neighboring locations in the high-dimensional embedding space, so as to achieve the constraint of the following alignment procession.

**Bidirectional Direct Alignment Block.** After the operation of the alignment constraint block, we apply the independent bidirectional direct alignment block to align the remapped text features  $f_{txt}^*$  with the point features  $f_{point}$  and the remapped image features  $f_{image}^*$  with the voxel features  $f_{voxel}$ , respectively.

For the text-to-point feature alignment process, first we use the features of  $n$ th point and its  $n_{nbr}$  neighboring points  $f_{points}^n \in \mathbb{R}^{(n_{nbr}+1) \times n_d}$  as Key and Value, and then the remapped text features  $f_{txt}^* \in \mathbb{R}^{1 \times n_d}$  are used as a Query for the cross-modal attention computation. The complete calculation procedure is shown in Equations (2) to (5):

$$Q = Linear_q^{\mathbb{R}^{1 \times n_d} \rightarrow \mathbb{R}^{(n_{nbr}+1) \times n_d}}(f_{txt}^*), \quad (2)$$

$$K, V = Linear_{k,v}^{\mathbb{R}^{(n_{nbr}+1) \times n_d} \rightarrow \mathbb{R}^{(n_{nbr}+1) \times n_d}}(f_{points}^n), \quad (3)$$

$$out^{txt} = \sum_{i=1}^{n_{nbr}+1} (softmax(Q \cdot K_i) \times V_i), \quad (4)$$

$$x_{txt}^{point_n} = Linear_{\mathbb{R}^{(n_{nbr}+1) \times n_d} \rightarrow \mathbb{R}^{1 \times n_d}}(out^{txt}), \quad (5)$$

where  $n_d$  is the dimension of features,  $Linear$  represents the linear layer operation and its superscript represents its input and output dimensions, and  $out^{txt}$  is the aggregated feature obtained after the whole attention computation process. Finally, the features are projected back to the dimension consistent with the input features through an additional linear layer to obtain the final enhanced text feature  $x_{txt}^{point_n}$  with the  $n$ th point.

After acquiring the point-augmented text features, we perform supplementary cross-modal attention computations to achieve bidirectional alignment between textual embeddings and point-level geometric features. In this attention computation, we use the features of the  $n$ th point  $x_{point}^n \in \mathbb{R}^{1 \times n_d}$  as Query and the corresponding text-enhanced features obtained from the same point  $x_{txt}^{point_n} \in \mathbb{R}^{1 \times n_d}$  as Key and Value. Thus, similar to the computational process described above, the enhanced text features  $x_{txt}^{point_n}$  is used again to enhance the features of the point  $f_{point}^n$ , thus completing the bidirectional alignment process between the text features and the point features, and generating point features  $f_{point}^*$  that align the text input.

Bidirectional direct alignment between voxel features  $f_{voxel}$  and remapped image features  $f_{image}^*$  is similar to the above process, getting voxel features  $f_{voxel}^*$  that align the image input. Then we concatenate the features of the corresponding voxel for each 3D point according to the correspondence between the 3D point and the 3D voxel to get the alignment features  $f_{align}$  of each 3D point.

### 3.3. Memory Module for Feature Pairs

Current datasets are often plagued by imbalanced training sample distributions, further complicated by the inherent intra-class divergence in texture and contextual features across objects of the same category. The above problems lead to the fact that different objects of the same category tend to be recognized as different categories, and the accuracy of objects with small sample sizes would be lower.

In order to solve the above problems, we propose a Memory Module as shown in Figure 3b. This module is set up on the thread that generates the final interactive segmentation results from the detection results, and is used to store high-confidence, in other words, low-loss, visual-textual feature pairs to constrain the binary classifier that generates the segmentation results.

The inputs to this module are the text features of each training scene and the features of the 3D points in the bounding box after processing by the detection head, firstly these two features are stored in the text memory bank and visual memory bank together with the corresponding features of the previously trained scenes in the training order.

Then we concatenate the corresponding elements of the two memory banks to obtain the feature-pairs memory bank. In addition, we assign a weight to each feature-pair element to generate a weighted feature-pairs memory bank, and the corresponding weight is inversely proportional to the loss of the corresponding scene of the feature-pair in the output of the segmentation mask.

Upon storing the data from the current training scene into the aforementioned memory banks, we dynamically retrieve prior knowledge by leveraging the features of the current scenario as Query and all stored features in the corresponding memory bank as Key and Value. Specifically, we sequentially conduct self-attention operations over the text memory bank and the weighted feature-pairs memory bank to enable adaptive cross-modal fusion. Then, we take the result of self-attention computation of text features as Query, and the result of self-attention computation of feature-pairs as Key and Value, and perform an additional computation of cross-attention. After the above three attention computations, we input the features into a binary classifier to generate the final mask for the interactive segmentation task. In addition, as described above, the binary cross-entropy loss of this binary classifier is used to weight the current feature-pair to update the impact of the it on the memory bank, thus further optimizing the training of the binary classifier.

### 3.4. Object Function

The objective function of the overall network training process is mainly divided into the following parts: one part is the detection loss and segmentation loss used for the whole network training process as shown in Equation (6), the detection loss consists of Smooth L1 Loss and weighted cross-entropy loss, and the segmentation loss consists of a binary cross-entropy loss. The other part is a symmetric cross-entropy loss function used only for the training process of the Direct Cross-Modal Alignment module. The above two parts of the objective function constitute that of the whole network, as shown in Equation (7). Detailed formulas for each part of the objective function are shown below.

$$\begin{aligned} \mathcal{L}_{task} &= \alpha \mathcal{L}_{det} + \beta \mathcal{L}_{seg} \\ &= \alpha \mathcal{L}_{smoothL1} + \alpha \mathcal{L}_{WCE} + \beta \mathcal{L}_{BCE}, \end{aligned} \quad (6)$$

$$\mathcal{L}_{all} = \mathcal{L}_{task} + \mathcal{L}_{SCE}. \quad (7)$$

As mentioned above, the objective function of our network consists of the detection loss  $\mathcal{L}_{det}$  and segmentation loss  $\mathcal{L}_{seg}$  for training the main network as shown in Equation (8) and the loss  $\mathcal{L}_{DCMA}$  for training the Direct Cross-Modal Alignment module as shown in Equation (9). We apply Smooth L1 loss as well as weighted cross-entropy loss

to construct the detection loss which are shown in Equations (10) and (11). For segmentation loss, we use a binary cross-entropy loss function as shown in Equation (12).

$$\begin{aligned}\mathcal{L}_{task} &= \alpha\mathcal{L}_{det} + \beta\mathcal{L}_{seg} \\ &= \alpha\mathcal{L}_{smoothL1} + \alpha\mathcal{L}_{WCE} + \beta\mathcal{L}_{BCE},\end{aligned}\quad (8)$$

$$\mathcal{L}_{smoothL1}(y, \hat{y}) = \begin{cases} 0.5(\hat{y} - y)^2/\epsilon, & \text{if } |\hat{y} - y| < \epsilon \\ |\hat{y} - y| - 0.5\epsilon, & \text{otherwise} \end{cases}, \quad (9)$$

$$\mathcal{L}_{WCE} = -\frac{1}{N} \sum_{i=1}^N \sum_{c=1}^C w_c \cdot y_{i,c} \log(p_{i,c}^{wce}), \quad (10)$$

$$\begin{aligned}\mathcal{L}_{BCE} &= -\frac{1}{N} \sum_{i=1}^N [y_i \log(p_i^{bce}) + (1 - y_i) \log(1 - p_i^{bce})], \\ &\quad (11)\end{aligned}$$

$$\begin{aligned}\mathcal{L}_{DCMA} &= \mathcal{L}_{SCE} \\ &= \gamma \cdot \left( -\sum_{i=1}^C y_i \log(p_i^{sce}) \right) + \\ &\quad \delta \cdot \left( -\sum_{i=1}^C p_i^{sce} \log(y_i) \right),\end{aligned}\quad (12)$$

where  $y$  is the true value,  $\hat{y}$  is the predicted value,  $\epsilon$  is a smoothing threshold parameter,  $N$  is the number of samples,  $C$  is the total number of categories,  $y_{i,c}$  is the true one-hot label of the  $i$ th sample,  $p_{i,c}^{wce}$  is the predicted probability of the  $i$ th sample for category  $c$ ,  $w_c$  is the weight of category  $c$ ,  $y_i$  is the true 0 or 1 label of the  $i$ th sample,  $p_{i,c}^{bce}$  is the probability that the  $i$ th sample is predicted to be the positive class, and  $p_{i,c}^{sce}$  is the predicted probability distribution of the  $i$ th sample.

## 4. Experiments

In this section, we first provide an overview of the experimental settings in Section 4.1. We then present the 3D instruction and referring segmentation results in Sections 4.2 and 4.3, respectively. After that, we conduct 3D semantic segmentation experiments in Section 4.4. Furthermore, we showcase the extensive ablation study in Section 4.5.

Method	Acc	mIoU
ReferIt3D [1]	11.7	6.4
ScanRefer [4]	12.0	6.9
TGNN [14]	12.9	7.1
BUTD-DETR [15]	16.3	10.9
EDA [49]	16.6	12.1
M3DRef-CLIP [54]	18.1	12.8
SegPoint [12]	31.6	<u>27.5</u>
Ours*	<u>32.3</u>	27.2
Ours	<b>34.1</b>	<b>28.4</b>

Table 1. 3D instruction segmentation results on Instruct3D [12]. \* denotes our method removing the proposed Memory Module.

### 4.1. Experimental Settings

**Datasets.** The network we proposed can be applied to a variety of downstream tasks of point cloud segmentation. In the experiment, we selected 3D instruction, 3D referring and 3D semantic segmentation tasks to test the network. For the 3D instruction segmentation, we use Instruct3D [12] based on ScanNet++ [51]; for the 3D referring segmentation task, we use ScanRefer [4] based on ScanNet [8]; in addition, for the semantic segmentation task, we chose a commonly used indoor large-scene dataset, S3DIS [2], and an outdoor large-scene dataset, SemanticKITTI [3].

**Instruct3D** [12] contains 280 scenarios from the ScanNet++ [51] dataset, each containing about 10 segmentation instructions containing functional information about the target category, resulting in 2,565 instruction point cloud pairs. The training and validation sets of this dataset contain 2,052 and 513 question-answer pairs, respectively.

**ScanRefer** [4] is based on ScanNet [8], in which 800 unique indoor environments are annotated with a total of 51,583 descriptions containing explicit target object category words, of which the training, validation, and test sets contain 36,665, 9,508, and 5,410 annotations, respectively. Since each of the annotated descriptions in this dataset has the scene id and object id of the corresponding object, the point cloud of the corresponding target object can be found in the ScanNet dataset, and the text-point cloud question-answer pairs can be further obtained.

**S3DIS** [2] contains 272 scene data from six different indoor regions containing 13 common indoor categories of structural elements with movable objects. In our experiment we take as text input a query statement containing all the category words of this dataset, such as ‘*Please segment the masks of all the categories in this point cloud in order and output separate masks for each category in the following category order: {category1}, {category2}, ...*’, and then our model outputs the category names and corresponding 3D masks with the order of the categories in the text input.

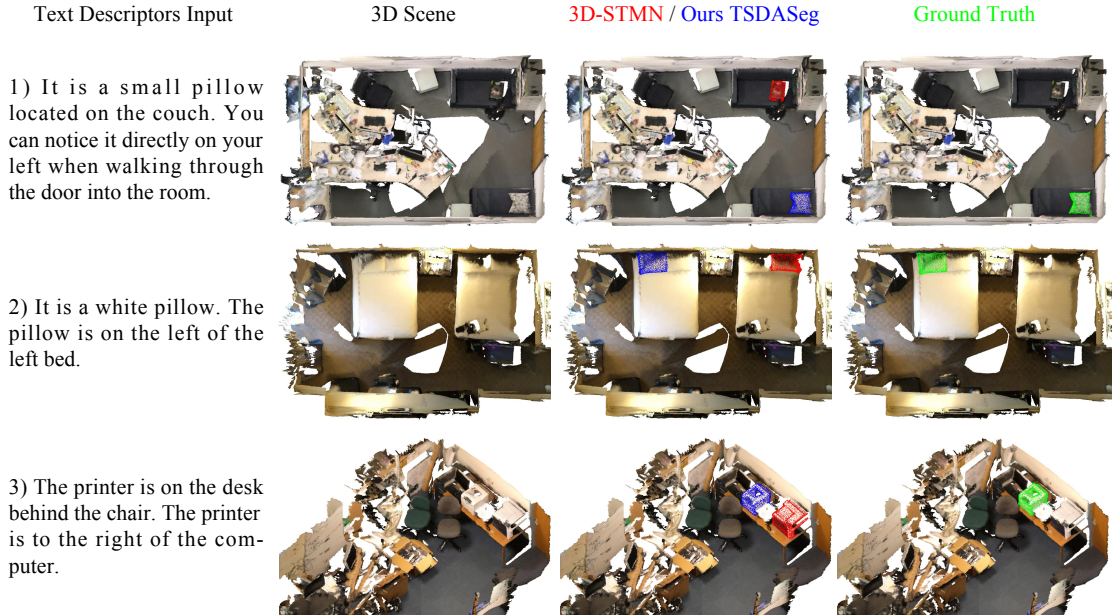


Figure 4. Qualitative results of 3D referring segmentation experiment on ScanRefer [4]. In the visualization results, the blue masks denote the segmentation outputs from our proposed TSDASeg, the red masks represent the predictions of the 3D-STMN [45], and the green masks indicate the ground truth annotations.

**SemanticKITTI** [3] consists of 22 point cloud sequences obtained from in-vehicle acquisition devices, where sequences 00 to 07 and 09, 10 are used for training, sequence 08 is used for validation, and sequences 11 to 21 are used for testing. For the experiment the input text settings are the same as in the previous dataset S3DIS [2].

**Metrics.** Following most of the existing studies on 3D segmentation, we adopt the mean Intersection-over-Union (mIoU), which is the average of all point cloud scene IoUs, as the main evaluation metric. In addition, in the experiments on the Instruct3D [12] dataset, we use the same accuracy (Acc) from SegPoint [12] to evaluate whether the model can accurately identify targets with IoU greater than 0.5. And in the experiments on S3DIS [2] dataset, we additionally use Overall Accuracy (OA), Mean Accuracy (mAcc) as evaluation metrics. The best indicators are highlighted in **bold** and the next best indicators are underlined.

**Implementation Details.** Experiments are implemented on a server equipped with four Nvidia V100 (32G  $\times$  4 GPU memory). Consistent with PTv3 [47], we use the AdamW optimizer with a cosine scheduler during training and set 1% of the training process as a warm-up. We set the initial learning rate and weight decay to 0.005, 0.05 and 0.002, 0.005 for indoor and outdoor scenes, respectively. In addition, the number of training epochs was set to 500 and 100 for the indoor and outdoor scenes, accordingly.

## 4.2. Experiments on 3D Instruction Segmentation

We present the performance on 3D instruction segmentation task of TSDASeg and SOTA methods in Table 1. In the Instruct3D [12] experiment, TSDASeg achieved excellent results, outperforming the SOTA method in both Acc and mIoU evaluation metrics. Even when not incorporating our proposed Memory Module for storing high-confidence text-visual query pairs, our method has a competitive level of accuracy compared to the best existing method, SegPoint [12]. Compare the last three rows of data in the table, our method without the Memory Module is 0.7% ahead of SegPoint [12] in Acc while only 0.3% behind in mIoU, and our full method is 2.5% and 0.9% ahead of SegPoint [12] in Acc and mIoU. These results show that our method has a strong text comprehension and reasoning ability.

## 4.3. Experiments on 3D Referring Segmentation

We showcase the performance on 3D referring segmentation task of TSDASeg and SOTA methods in Table 2. In the ScanRefer [4] experiment, our TSDASeg achieves superior results, with at least 0.5% mIoU improvement over SOTA methods. This demonstrates that our method not only has strong comprehension and inference ability, but also has text-visual association construction ability, which means that it can query the distribution of the corresponding objects in 3D space based on the explicit text words.

Moreover, we also conduct qualitative results of our method on the validation set of ScanRefer [4], as shown in

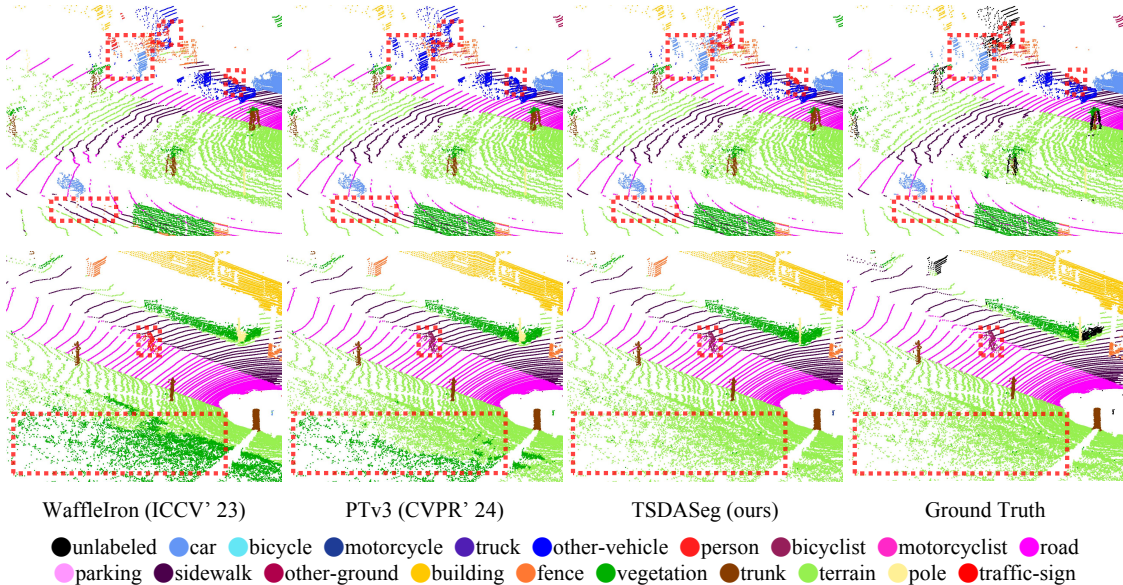


Figure 5. Qualitative results of 3D semantic segmentation experiment on SemanticKITTI [3].

Method	mIoU
TGNN [14]	27.8
BUTD-DETR [15]	35.4
EDA [49]	36.2
M3DRef-CLIP [54]	35.7
X-RefSeg3D [35]	29.9
3D-STMN [45]	39.5
RefMask3D [11]	44.8
SegPoint [12]	41.7
<b>Ours</b>	<b>45.3</b>

Table 2. 3D referring segmentation results on ScanRefer [4].

Method	OA	mAcc	mIoU
PointNet [32]	-	49.0	41.1
KPConv [40]	-	72.8	67.1
PCT [10]	-	67.7	61.3
ST [17]	91.5	78.1	71.0
SPT [37]	89.5	77.3	68.9
PTv2 [46]	91.6	78.0	72.6
PTv3 [47]	-	-	73.4
PTv3+PPT [47, 48]	<u>92.0</u>	<u>80.1</u>	<u>74.7</u>
<b>Ours</b>	<b>93.2</b>	<b>84.5</b>	<b>75.8</b>

Table 3. Indoor 3D semantic segmentation results on S3DIS [2].

Figure 4. It can be seen that our method has stronger individual discrimination and recognition ability when there are

Method	mIoU
SphereFormer [18]	67.8
WaffleIron [31]	68.0
2DPASS [50]	69.3
PTv2 [46]	70.3
OA-CNNs [30]	70.6
PPT+SparseUNet [48]	71.4
PTv3+PPT [47, 48]	<u>72.3</u>
<b>Ours</b>	<b>73.5</b>

Table 4. Outdoor 3D semantic segmentation results on the validation set of SemanticKITTI [3].

multiple similar objects of the target category in the same space. Compared to the comparison method 3D-STMN [45], our performance is exceptionally outstanding in multiple scenes. For scenes with multiple objects of the same category in close distance and when the text descriptions are long and complex, 3D-STMN [45] has a higher probability of taking non-target objects as outputs yielding incorrect target responses. In contrast, our TSDASeg can better understand and reason to get the correct target object of the text description. This is also attributed to the rich knowledge of text-visual query mapping that the proposed Memory Module brings to the overall network.

#### 4.4. Experiments on 3D Semantic Segmentation

We summarize the performance on 3D semantic segmentation task of TSDASeg and SOTA methods in Table 3 and Table 4. Experiments on the S3DIS [2] Area 5 (Table 3)

Method	mIoU	$\Delta$
w/o MMFP and DCMA	26.4	+0.0
w/o Memory Module for Feature Pairs	27.2	+0.8
w/o Direct Cross-Modal Alignment	27.5	+1.1
w/ all	28.4	+2.0

Table 5. Ablation study of different proposed modules on Instruct3D [12].

our method achieves a superior result, outperforming the method [47, 48] that using multiple datasets as training data in terms of all three overall accuracy metrics. Experiments on the SemanticKITTI validation set (Table 4) show that TSDASeg has an accuracy improvement of at least 1.2% in mIoU compared to existing methods. This can prove that allowing the 3D segmentation network to perceive the category information in the scene in advance during the feature processing stage helps its segmentation accuracy to be improved. For a fair comparison, our method is trained using only the data in the corresponding dataset in our experiments, and no data from additional datasets are added to augment the training samples.

Furthermore, we also conduct qualitative results of our method on the SemanticKITTI [3] validation set, as shown in Figure 5. It can be seen that our method has better segmentation in the region labelled with red boxes, which indicates that our method has stronger recognition ability for similar categories (different categories of terrain, different categories of carriers, etc.). This is because our method is able to have the perception of specific category information in the scene compared to existing commonly used 3D semantic segmentation methods, and the knowledge of mapping category words to visual features from the proposed Memory Module also enables the network to better distinguish different similar categories of objects.

#### 4.5. Ablation Experiments

Compare the last two rows of data shown in Table 1, the method with our proposed Memory Module has an accuracy improvement of 1.8% and 1.2% in Acc and mIoU, respectively, which shows the importance of the proposed Memory Module in improving the network’s ability to understand text-visual feature correspondences.

Table 5 summarizes the impact on each part of our proposed module, Direct Cross-Modal Alignment and Memory Module for Feature Pairs, on Instruct3D [12]. The experimental results demonstrate that network accuracy achieves enhancements of 0.8%, 1.1%, and 2.0% under three conditions: (a) introducing the Direct Cross-Modal Alignment module, (b) deploying the Memory Module for Feature Pairs independently, and (c) combining both modules, re-

spectively. The proposed method mitigates the negative impacts caused by error accumulation and 2D-3D coordinate mapping distortions in conventional alignment approaches through two strategic mechanisms: (1) explicitly bridging 3D features with multimodal representations via direct alignment, and (2) integrating text-2D feature correlations by contrastive learning as constraints to regulate the 3D feature alignment process. Meanwhile, our proposed Memory Module can further constrain the output process from 3D bounding boxes to segmentation results, and store high-confidence text-to-vision mapping relations to enhance the text-to-vision inference capability of the network. The combination of the above two modules can further improve the network’s accuracy for interactive segmentation tasks.

## 5. Conclusions

We propose a two-stage interactive point cloud segmentation model with detection followed by segmentation. In order to avoid the effect of computational errors in internal and external parameters, we design a Direct Cross-Modal Alignment module that directly aligns 3D features with text/image. In addition, we propose a Memory Module that stores the mapping of text queries and visual features with high confidence during training in order to constrain the process from the 3D bounding boxes to the final interactive segmentation results, which can improve the processing accuracy of the network. Satisfactory accuracy results are obtained in the experiments on a variety of different segmentation downstream tasks, demonstrating the effectiveness and robustness of the proposed method.

## References

- [1] Panos Achlioptas, Ahmed Abdelreheem, Fei Xia, Mohamed Elhoseiny, and Leonidas Guibas. Referit3d: Neural listeners for fine-grained 3d object identification in real-world scenes. In *Proceedings of the European Conference on Computer Vision (ECCV)*, pages 422–440, 2020. 3, 6
- [2] Iro Armeni, Ozan Sener, Amir R. Zamir, Helen Jiang, Ioannis Brilakis, Martin Fischer, and Silvio Savarese. 3d semantic parsing of large-scale indoor spaces. In *2016 IEEE Conference on Computer Vision and Pattern Recognition (CVPR)*, pages 1534–1543, 2016. 6, 7, 8
- [3] Jens Behley, Martin Garbade, Andres Milioto, Jan Quenzel, Sven Behnke, Cyrill Stachniss, and Jurgen Gall. Semantickitti: A dataset for semantic scene understanding of lidar sequences. In *Proceedings of the IEEE/CVF International Conference on Computer Vision (ICCV)*, pages 9297–9307, 2019. 6, 7, 8, 9
- [4] Dave Zhenyu Chen, Angel X. Chang, and Matthias Nießner. Scanrefer: 3d object localization in rgb-d scans using natural language. In *Proceedings of the European Conference on Computer Vision (ECCV)*, pages 202–221, 2020. 3, 6, 7, 8
- [5] Xuechao Chen, Shuangjie Xu, Xiaoyi Zou, Tongyi Cao, Dityan Yeung, and Lu Fang. Svqnet: Sparse voxel-adjacent

- query network for 4d spatio-temporal lidar semantic segmentation. In *2023 IEEE/CVF International Conference on Computer Vision (ICCV)*, pages 8535–8544, 2023. 2
- [6] Christopher Choy, JunYoung Gwak, and Silvio Savarese. 4d spatio-temporal convnets: Minkowski convolutional neural networks. In *Proceedings of the IEEE/CVF conference on computer vision and pattern recognition*, pages 3075–3084, 2019. 2
- [7] Angela Dai and Matthias Nießner. 3dmv: Joint 3d-multi-view prediction for 3d semantic scene segmentation. In *Proceedings of the European Conference on Computer Vision (ECCV)*, pages 452–468, 2018. 2
- [8] Angela Dai, Angel X. Chang, Manolis Savva, Maciej Halber, Thomas Funkhouser, and Matthias Nießner. Scannet: Richly-annotated 3d reconstructions of indoor scenes. In *2017 IEEE Conference on Computer Vision and Pattern Recognition (CVPR)*, pages 2432–2443, 2017. 6
- [9] Benjamin Graham, Martin Engelcke, and Laurens Van Der Maaten. 3d semantic segmentation with submanifold sparse convolutional networks. In *Proceedings of the IEEE conference on computer vision and pattern recognition*, pages 9224–9232, 2018. 2
- [10] Meng-Hao Guo, Jun-Xiong Cai, Zheng-Ning Liu, Tai-Jiang Mu, Ralph R Martin, and Shi-Min Hu. Pct: Point cloud transformer. *Computational Visual Media*, 7:187–199, 2021. 2, 8
- [11] Shuting He and Henghui Ding. Refmask3d: Language-guided transformer for 3d referring segmentation. In *Proceedings of the 32nd ACM International Conference on Multimedia*, page 8316–8325, 2024. 3, 8
- [12] Shuting He, Henghui Ding, Xudong Jiang, and Bihan Wen. Segpoint: Segment any point cloud via large language model. In *Proceedings of the European Conference on Computer Vision (ECCV)*, pages 349–367, 2024. 1, 3, 6, 7, 8, 9
- [13] Qingyong Hu, Bo Yang, Linhai Xie, Stefano Rosa, Yulan Guo, Zhihua Wang, Niki Trigoni, and Andrew Markham. Learning semantic segmentation of large-scale point clouds with random sampling. *IEEE Transactions on Pattern Analysis and Machine Intelligence*, 44(11):8338–8354, 2021. 2
- [14] Pin-Hao Huang, Han-Hung Lee, Hwann-Tzong Chen, and Tyng-Luh Liu. Text-guided graph neural networks for referring 3d instance segmentation. In *Thirty-fifth AAAI Conference on Artificial Intelligence*, pages 1610–1618, 2021. 3, 6, 8
- [15] Ayush Jain, Nikolaos Gkanatsios, Ishita Mediratta, and Katerina Fragkiadaki. Bottom up top down detection transformers for language grounding in images and point clouds. In *Proceedings of the European Conference on Computer Vision (ECCV)*, pages 417–433, 2022. 3, 6, 8
- [16] Maximilian Jaritz, Tuan-Hung Vu, Raoul de Charette, Emilie Wirbel, and Patrick Pérez. xmuda: Cross-modal unsupervised domain adaptation for 3d semantic segmentation. In *Proceedings of the IEEE/CVF conference on computer vision and pattern recognition*, pages 12605–12614, 2020. 2
- [17] Xin Lai, Jianhui Liu, Li Jiang, Liwei Wang, Hengshuang Zhao, Shu Liu, Xiaojuan Qi, and Jiaya Jia. Stratified transformer for 3d point cloud segmentation. In *Proceedings of the IEEE/CVF conference on computer vision and pattern recognition*, pages 8500–8509, 2022. 2, 8
- [18] Xin Lai, Yukang Chen, Fanbin Lu, Jianhui Liu, and Jiaya Jia. Spherical transformer for lidar-based 3d recognition. In *Proceedings of the IEEE/CVF Conference on Computer Vision and Pattern Recognition (CVPR)*, pages 17545–17555, 2023. 8
- [19] Xin Lai, Yuhui Yuan, Ruihang Chu, Yukang Chen, Han Hu, and Jiaya Jia. Mask-attention-free transformer for 3d instance segmentation. In *2023 IEEE/CVF International Conference on Computer Vision (ICCV)*, pages 3670–3680, 2023. 2
- [20] Felix Järemo Lawin, Martin Danelljan, Patrik Tosteberg, Goutam Bhat, Fahad Shahbaz Khan, and Michael Felsberg. Deep projective 3d semantic segmentation. In *Computer Analysis of Images and Patterns: 17th International Conference, CAIP 2017, Ystad, Sweden, August 22-24, 2017, Proceedings, Part I 17*, pages 95–107, 2017. 2
- [21] Chade Li, Pengju Zhang, Bo Liu, Hao Wei, and Yihong Wu. Feast-mamba: Feature and spatial aware mamba network with bidirectional orthogonal fusion for cross-modal point cloud segmentation. In *Thirty-ninth AAAI Conference on Artificial Intelligence*, 2025. 2
- [22] Guohao Li, Matthias Muller, Ali Thabet, and Bernard Ghanem. Deepgcns: Can gcns go as deep as cnns? In *Proceedings of the IEEE/CVF international conference on computer vision*, pages 9267–9276, 2019. 2
- [23] Miaoyu Li, Yachao Zhang, Xu Ma, Yanyun Qu, and Yun Fu. Bev-dg: Cross-modal learning under bird’s-eye view for domain generalization of 3d semantic segmentation. In *2023 IEEE/CVF International Conference on Computer Vision (ICCV)*, pages 11598–11608, 2023. 2
- [24] Yangyan Li, Rui Bu, Mingchao Sun, Wei Wu, Xinhan Di, and Baoquan Chen. Pointcnn: Convolution on x-transformed points. In *Proceedings of the 32nd International Conference on Neural Information Processing Systems*, page 828–838, 2018. 2
- [25] Youquan Liu, Lingdong Kong, Jun Cen, Runnan Chen, Wenwei Zhang, Liang Pan, Kai Chen, and Ziwei Liu. Segment any point cloud sequences by distilling vision foundation models. In *Proceedings of the 37th International Conference on Neural Information Processing Systems*, pages 37193–37229, 2023. 1, 2
- [26] Jiahao Lu, Jiacheng Deng, Chuxin Wang, Jianfeng He, and Tianzhu Zhang. Query refinement transformer for 3d instance segmentation. In *2023 IEEE/CVF International Conference on Computer Vision (ICCV)*, pages 18470–18480, 2023. 2
- [27] Yuhang Lu, Qi Jiang, Runnan Chen, Yuenan Hou, Xinge Zhu, and Yuexin Ma. See more and know more: Zero-shot point cloud segmentation via multi-modal visual data. In *2023 IEEE/CVF International Conference on Computer Vision (ICCV)*, pages 21617–21627, 2023. 2
- [28] Chungyun Park, Yoonwoo Jeong, Minsu Cho, and Jaesik Park. Fast point transformer. In *Proceedings of the IEEE/CVF conference on computer vision and pattern recognition*, pages 16949–16958, 2022. 2

- [29] Jinyoung Park, Sanghyeok Lee, Sihyeon Kim, Yunyang Xiong, and Hyunwoo J Kim. Self-positioning point-based transformer for point cloud understanding. In *Proceedings of the IEEE/CVF conference on computer vision and pattern recognition*, pages 21814–21823, 2023. 2
- [30] Bohao Peng, Xiaoyang Wu, Li Jiang, Yukang Chen, Hengshuang Zhao, Zhuotao Tian, and Jiaya Jia. Oa-cnns: Omni-adaptive sparse cnns for 3d semantic segmentation. In *Proceedings of the IEEE/CVF Conference on Computer Vision and Pattern Recognition (CVPR)*, pages 21305–21315, 2024. 8
- [31] Gilles Puy, Alexandre Boulch, and Renaud Marlet. Using a waffle iron for automotive point cloud semantic segmentation. In *2023 IEEE/CVF International Conference on Computer Vision (ICCV)*, pages 3356–3366, 2023. 2, 8
- [32] Charles R. Qi, Hao Su, Kaichun Mo, and Leonidas J Guibas. Pointnet: Deep learning on point sets for 3d classification and segmentation. In *Proceedings of the IEEE conference on computer vision and pattern recognition*, pages 652–660, 2017. 2, 8
- [33] Charles R. Qi, Li Yi, Hao Su, and Leonidas J. Guibas. Pointnet++: deep hierarchical feature learning on point sets in a metric space. In *Proceedings of the 31st International Conference on Neural Information Processing Systems*, page 5105–5114, 2017. 2
- [34] Zhangyang Qi, Ye Fang, Zeyi Sun, Xiaoyang Wu, Tong Wu, Jiaqi Wang, Dahua Lin, and Hengshuang Zhao. Gpt4point: A unified framework for point-language understanding and generation. In *Proceedings of the IEEE/CVF Conference on Computer Vision and Pattern Recognition (CVPR)*, pages 26417–26427, 2024. 1
- [35] Zhipeng Qian, Yiwei Ma, Jiayi Ji, and Xiaoshuai Sun. X-refseg3d: Enhancing referring 3d instance segmentation via structured cross-modal graph neural networks. In *Thirty-Eighth AAAI Conference on Artificial Intelligence*, pages 4551–4559, 2024. 3, 8
- [36] Alec Radford, Jong Wook Kim, Chris Hallacy, Aditya Ramesh, Gabriel Goh, Sandhini Agarwal, Girish Sastry, Amanda Askell, Pamela Mishkin, Jack Clark, Gretchen Krueger, and Ilya Sutskever. Learning transferable visual models from natural language supervision. In *Proceedings of the 38th International Conference on Machine Learning*, pages 8748–8763, 2021. 1
- [37] Damien Robert, Hugo Raguét, and Loïc Landrieu. Efficient 3d semantic segmentation with superpoint transformer. In *Proceedings of the IEEE/CVF International Conference on Computer Vision*, pages 17195–17204, 2023. 2, 8
- [38] Damien Robert, Hugo Raguét, and Loïc Landrieu. Scalable 3d panoptic segmentation as superpoint graph clustering. In *2024 International Conference on 3D Vision (3DV)*, pages 179–189, 2024. 2
- [39] Jules Sanchez, Jean-Emmanuel Deschaud, and François Goulette. Domain generalization of 3d semantic segmentation in autonomous driving. In *2023 IEEE/CVF International Conference on Computer Vision (ICCV)*, pages 18031–18041, 2023. 2
- [40] Hugues Thomas, Charles R Qi, Jean-Emmanuel Deschaud, Beatriz Marcotegui, François Goulette, and Leonidas J Guibas. Kpconv: Flexible and deformable convolution for point clouds. In *Proceedings of the IEEE/CVF international conference on computer vision*, pages 6411–6420, 2019. 2, 8
- [41] Hugo Touvron, Louis Martin, Kevin R. Stone, Peter Albert, Amjad Almahairi, Yasmine Babaei, Nikolay Bashlykov, Soumya Batra, Prajjwal Bhargava, Shruti Bhosale, Daniel M. Bikel, Lukas Blecher, Cristian Cantón Ferrer, Moya Chen, Guillem Cucurull, David Esiobu, Jude Fernandes, Jeremy Fu, Wenyin Fu, Brian Fuller, Cynthia Gao, Vedanuj Goswami, Naman Goyal, Anthony S. Hartshorn, Saghar Hosseini, Rui Hou, Hakan Inan, Marcin Kardas, Viktor Kerkez, Madian Khabsa, Isabel M. Kloumann, A. V. Korenev, Punit Singh Koura, Marie-Anne Lachaux, Thibaut Lavril, Jenya Lee, Diana Liskovich, Yinghai Lu, Yuning Mao, Xavier Martinet, Todor Mihaylov, Pushkar Mishra, Igor Molybog, Yixin Nie, Andrew Poulton, Jeremy Reizenstein, Rashi Rungta, Kalyan Saladi, Alan Schelten, Ruan Silva, Eric Michael Smith, R. Subramanian, Xia Tan, Binh Tang, Ross Taylor, Adina Williams, Jian Xiang Kuan, Puxin Xu, Zhengxu Yan, Iliyan Zarov, Yuchen Zhang, Angela Fan, Melissa Hall Melanie Kambadur, Sharan Narang, Aurélien Rodriguez, Robert Stojnic, Sergey Edunov, and Thomas Scialom. Llama 2: Open foundation and fine-tuned chat models. *arXiv preprint arXiv:2307.09288*, 2023. 3
- [42] Ardian Umam, Cheng-Kun Yang, Min-Hung Chen, Jen-Hui Chuang, and Yen-Yu Lin. Partdistill: 3d shape part segmentation by vision-language model distillation. In *2024 IEEE/CVF Conference on Computer Vision and Pattern Recognition (CVPR)*, pages 3470–3479, 2024. 1
- [43] Peng-Shuai Wang. Octformer: Octree-based transformers for 3d point clouds. *ACM Transactions on Graphics (TOG)*, 42(4):1–11, 2023. 2
- [44] Bichen Wu, Alvin Wan, Xiangyu Yue, and Kurt Keutzer. Squeezeseg: Convolutional neural nets with recurrent crf for real-time road-object segmentation from 3d lidar point cloud. In *2018 IEEE international conference on robotics and automation (ICRA)*, pages 1887–1893, 2018. 2
- [45] Changli Wu, Yiwei Ma, Qi Chen, Haowei Wang, Gen Luo, Jiayi Ji, and Xiaoshuai Sun. 3d-stmn: dependency-driven superpoint-text matching network for end-to-end 3d referring expression segmentation. In *Thirty-Eighth AAAI Conference on Artificial Intelligence*, pages 5940–5948, 2024. 3, 7, 8
- [46] Xiaoyang Wu, Yixing Lao, Li Jiang, Xihui Liu, and Hengshuang Zhao. Point transformer v2: Grouped vector attention and partition-based pooling. In *Proceedings of the 36th International Conference on Neural Information Processing Systems*, pages 33330–33342, 2022. 2, 8
- [47] Xiaoyang Wu, Li Jiang, Peng-Shuai Wang, Zhijian Liu, Xihui Liu, Yu Qiao, Wanli Ouyang, Tong He, and Hengshuang Zhao. Point transformer v3: Simpler faster stronger. In *Proceedings of the IEEE/CVF Conference on Computer Vision and Pattern Recognition (CVPR)*, pages 4840–4851, 2024. 2, 7, 8, 9
- [48] Xiaoyang Wu, Zhuotao Tian, Xin Wen, Bohao Peng, Xihui Liu, Kaicheng Yu, and Hengshuang Zhao. Towards large-scale 3d representation learning with multi-dataset point

- prompt training. In *Proceedings of the IEEE/CVF Conference on Computer Vision and Pattern Recognition (CVPR)*, pages 19551–19562, 2024. [8](#), [9](#)
- [49] Yanmin Wu, Xinhua Cheng, Renrui Zhang, Zesen Cheng, and Jian Zhang. Eda: Explicit text-decoupling and dense alignment for 3d visual grounding. In *2023 IEEE/CVF Conference on Computer Vision and Pattern Recognition (CVPR)*, pages 19231–19242, 2023. [3](#), [6](#), [8](#)
- [50] Xu Yan, Jiantao Gao, Chaoda Zheng, Chao Zheng, Ruimao Zhang, Shuguang Cui, and Zhen Li. 2dpass: 2d priors assisted semantic segmentation on lidar point clouds. In *Proceedings of the European Conference on Computer Vision (ECCV)*, pages 677–695, 2022. [8](#)
- [51] Chandan Yeshwanth, Yueh-Cheng Liu, Matthias Nießner, and Angela Dai. Scannet++: A high-fidelity dataset of 3d indoor scenes. In *Proceedings of the IEEE/CVF International Conference on Computer Vision (ICCV)*, pages 12–22, 2023. [6](#)
- [52] Renrui Zhang, Ziyu Guo, Wei Zhang, Kunchang Li, Xupeng Miao, Bin Cui, Yu Qiao, Peng Gao, and Hongsheng Li. Pointclip: Point cloud understanding by clip. In *2022 IEEE/CVF Conference on Computer Vision and Pattern Recognition (CVPR)*, pages 8542–8552, 2022. [1](#), [2](#)
- [53] Yang Zhang, Zixiang Zhou, Philip David, Xiangyu Yue, Zerong Xi, Boqing Gong, and Hassan Foroosh. Polarnet: An improved grid representation for online lidar point clouds semantic segmentation. In *Proceedings of the IEEE/CVF conference on computer vision and pattern recognition*, pages 9601–9610, 2020. [2](#)
- [54] Yiming Zhang, ZeMing Gong, and Angel X. Chang. Multi3drefer: Grounding text description to multiple 3d objects. In *Proceedings of the IEEE/CVF International Conference on Computer Vision (ICCV)*, pages 15225–15236, 2023. [3](#), [6](#), [8](#)
- [55] Hengshuang Zhao, Li Jiang, Jiaya Jia, Philip HS Torr, and Vladlen Koltun. Point transformer. In *Proceedings of the IEEE/CVF international conference on computer vision*, pages 16259–16268, 2021. [2](#)
- [56] Haoyu Zhen, Xiaowen Qiu, Peihao Chen, Jincheng Yang, Xin Yan, Yilun Du, Yining Hong, and Chuang Gan. 3D-VLA: A 3D vision-language-action generative world model. In *Proceedings of the 41st International Conference on Machine Learning*, pages 61229–61245, 2024. [1](#)